

Centrality dependence of $\pi^{+/-}$, $K^{+/-}$, p and \bar{p} production from $\sqrt{s_{NN}} = 130$ GeV Au + Au collisions at RHIC

K. Adcox,⁴⁰ S. S. Adler,³ N. N. Ajitanand,²⁷ Y. Akiba,¹⁴ J. Alexander,²⁷ L. Aphecetche,³⁴ Y. Arai,¹⁴ S. H. Aronson,³ R. Averbeck,²⁸ T. C. Awes,²⁹ K. N. Barish,⁵ P. D. Barnes,¹⁹ J. Barrette,²¹ B. Bassalleck,²⁵ S. Bathe,²² V. Baublis,³⁰ A. Bazilevsky,^{12,32} S. Belikov,^{12,13} F. G. Bellaiche,²⁹ S. T. Belyaev,¹⁶ M. J. Bennett,¹⁹ Y. Berdnikov,³⁵ S. Botelho,³³ M. L. Brooks,¹⁹ D. S. Brown,²⁶ N. Bruner,²⁵ D. Bucher,²² H. Buesching,²² V. Bumazhnov,¹² G. Bunce,^{3,32} J. Burward-Hoy,²⁸ S. Butsyk,^{28,30} T. A. Carey,¹⁹ P. Chand,² J. Chang,⁵ W. C. Chang,¹ L. L. Chavez,²⁵ S. Chernichenko,¹² C. Y. Chi,⁸ J. Chiba,¹⁴ M. Chiu,⁸ R. K. Choudhury,² T. Christ,²⁸ T. Chujo,^{3,39} M. S. Chung,^{15,19} P. Chung,²⁷ V. Cianciolo,²⁹ B. A. Cole,⁸ D. G. D'Enterria,³⁴ G. David,³ H. Delagrangé,³⁴ A. Denisov,¹² A. Deshpande,³² E. J. Desmond,³ O. Dietzsch,³³ B. V. Dinesh,² A. Drees,²⁸ A. Durum,¹² D. Dutta,² K. Ebisu,²⁴ Y. V. Efremenko,²⁹ K. El Chenawi,⁴⁰ H. En'yo,^{17,31} S. Esumi,³⁹ L. Ewell,³ T. Ferdousi,⁵ D. E. Fields,²⁵ S. L. Fokin,¹⁶ Z. Fraenkel,⁴² A. Franz,³ A. D. Frawley,⁹ S.-Y. Fung,⁵ S. Garpman,^{20,*} T. K. Ghosh,⁴⁰ A. Glenn,³⁶ A. L. Godoi,³³ Y. Goto,³² S. V. Greene,⁴⁰ M. Grosse Perdekamp,³² S. K. Gupta,² W. Guryñ,³ H.-Å. Gustafsson,²⁰ J. S. Haggerty,³ H. Hamagaki,⁷ A. G. Hansen,¹⁹ H. Hara,²⁴ E. P. Hartouni,¹⁸ R. Hayano,³⁸ N. Hayashi,³¹ X. He,¹⁰ T. K. Hemmick,²⁸ J. M. Heuser,²⁸ M. Hibino,⁴¹ J. C. Hill,¹³ D. S. Ho,⁴³ K. Homma,¹¹ B. Hong,¹⁵ A. Hoover,²⁶ T. Ichihara,^{31,32} K. Imai,^{17,31} M. S. Ippolitov,¹⁶ M. Ishihara,^{31,32} B. V. Jacak,^{28,32} W. Y. Jang,¹⁵ J. Jia,²⁸ B. M. Johnson,³ S. C. Johnson,^{18,28} K. S. Joo,²³ S. Kametani,⁴¹ J. H. Kang,⁴³ M. Kann,³⁰ S. S. Kapoor,² S. Kelly,⁸ B. Khachaturov,⁴² A. Khanzadeev,³⁰ J. Kikuchi,⁴¹ D. J. Kim,⁴³ H. J. Kim,⁴³ S. Y. Kim,⁴³ Y. G. Kim,⁴³ W. W. Kinnison,¹⁹ E. Kistenev,³ A. Kiyomichi,³⁹ C. Klein-Boesing,²² S. Klinksiek,²⁵ L. Kochenda,³⁰ V. Kochetkov,¹² D. Koehler,²⁵ T. Kohama,¹¹ D. Kotchetkov,⁵ A. Kozlov,⁴² P. J. Kroon,³ K. Kurita,^{31,32} M. J. Kweon,¹⁵ Y. Kwon,⁴³ G. S. Kyle,²⁶ R. Lacey,²⁷ J. G. Lajoie,¹³ J. Lauret,²⁷ A. Lebedev,^{13,16} D. M. Lee,¹⁹ M. J. Leitch,¹⁹ X. H. Li,⁵ Z. Li,^{6,31} D. J. Lim,⁴³ M. X. Liu,¹⁹ X. Liu,⁶ Z. Liu,⁶ C. F. Maguire,⁴⁰ J. Mahon,³ Y. I. Makdisi,³ V. I. Manko,¹⁶ Y. Mao,^{6,31} S. K. Mark,²¹ S. Markacs,⁸ G. Martinez,³⁴ M. D. Marx,²⁸ A. Masaike,¹⁷ F. Matathias,²⁸ T. Matsumoto,^{7,41} P. L. McGaughey,¹⁹ E. Melnikov,¹² M. Merschmeyer,²² F. Messer,²⁸ M. Messer,³ Y. Miake,³⁹ T. E. Miller,⁴⁰ A. Milov,⁴² S. Mioduszewski,^{3,36} R. E. Mischke,¹⁹ G. C. Mishra,¹⁰ J. T. Mitchell,³ A. K. Mohanty,² D. P. Morrison,³ J. M. Moss,¹⁹ F. Mühlbacher,²⁸ M. Muniruzzaman,⁵ J. Murata,³¹ S. Nagamiya,¹⁴ Y. Nagasaka,²⁴ J. L. Nagle,⁸ Y. Nakada,¹⁷ B. K. Nandi,⁵ J. Newby,³⁶ L. Nikkinen,²¹ P. Nilsson,²⁰ S. Nishimura,⁷ A. S. Nyanin,¹⁶ J. Nystrand,²⁰ E. O'Brien,³ C. A. Ogilvie,¹³ H. Ohnishi,^{3,11} I. D. Ojha,^{4,40} M. Ono,³⁹ V. Onuchin,¹² A. Oskarsson,²⁰ L. Österman,²⁰ I. Otterlund,²⁰ K. Oyama,^{7,38} L. Paffrath,^{3,*} A. P. T. Palounek,¹⁹ V. S. Pantuev,²⁸ V. Papavassiliou,²⁶ S. F. Pate,²⁶ T. Peitzmann,²² A. N. Petridis,¹³ C. Pinkenburg,^{3,27} R. P. Pisani,³ P. Pitukhin,¹² F. Plasil,²⁹ M. Pollack,^{28,36} K. Pope,³⁶ M. L. Purschke,³ I. Ravinovich,⁴² K. F. Read,^{29,36} K. Reygers,²² V. Riabov,^{30,35} Y. Riabov,³⁰ M. Rosati,¹³ A. A. Rose,⁴⁰ S. S. Ryu,⁴³ N. Saito,^{31,32} A. Sakaguchi,¹¹ T. Sakaguchi,^{7,41} H. Sako,³⁹ T. Sakuma,^{31,37} V. Samsonov,³⁰ T. C. Sangster,¹⁸ R. Santo,²² H. D. Sato,^{17,31} S. Sato,³⁹ S. Sawada,¹⁴ B. R. Schlei,¹⁹ Y. Schutz,³⁴ V. Semenov,¹² R. Seto,⁵ T. K. Shea,³ I. Shein,¹² T. -A. Shibata,^{31,37} K. Shigaki,¹⁴ T. Shiina,¹⁹ Y. H. Shin,⁴³ I. G. Sibiriyak,¹⁶ D. Silvermyr,²⁰ K. S. Sim,¹⁵ J. Simon-Gillo,¹⁹ C. P. Singh,⁴ V. Singh,⁴ M. Sivertz,³ A. Soldatov,¹² R. A. Soltz,¹⁸ S. Sorensen,^{29,36} P. W. Stankus,²⁹ N. Starinsky,²¹ P. Steinberg,⁸ E. Stenlund,²⁰ A. Ster,⁴⁴ S. P. Stoll,³ M. Sugioka,^{31,37} T. Sugitate,¹¹ J. P. Sullivan,¹⁹ Y. Sumi,¹¹ Z. Sun,⁶ M. Suzuki,³⁹ E. M. Takagui,³³ A. Taketani,³¹ M. Tamai,⁴¹ K. H. Tanaka,¹⁴ Y. Tanaka,²⁴ E. Taniguchi,^{31,37} M. J. Tannenbaum,³ J. Thomas,²⁸ J. H. Thomas,¹⁸ T. L. Thomas,²⁵ W. Tian,^{6,36} J. Tojo,^{17,31} H. Torii,^{17,31} R. S. Towell,¹⁹ I. Tserruya,⁴² H. Tsuruoka,³⁹ A. A. Tsvetkov,¹⁶ S. K. Tuli,⁴ H. Tydesjö,²⁰ N. Tyurin,¹² T. Ushiroda,²⁴ H. W. van Hecke,¹⁹ C. Velissaris,²⁶ J. Velkovska,²⁸ M. Velkovsky,²⁸ A. A. Vinogradov,¹⁶ M. A. Volkov,¹⁶ A. Vorobyov,³⁰ E. Vznuzdaev,³⁰ H. Wang,⁵ Y. Watanabe,^{31,32} S. N. White,³ C. Witzig,³ F. K. Wohn,¹³ C. L. Woody,³ W. Xie,^{5,42} K. Yagi,³⁹ S. Yokkaichi,³¹ G. R. Young,²⁹ I. E. Yushmanov,¹⁶ W. A. Zajc,⁸ Z. Zhang,²⁸ and S. Zhou⁶

(PHENIX Collaboration)

¹*Institute of Physics, Academia Sinica, Taipei 11529, Taiwan*

²*Bhabha Atomic Research Centre, Bombay 400 085, India*

³*Brookhaven National Laboratory, Upton, NY 11973-5000, USA*

⁴*Department of Physics, Banaras Hindu University, Varanasi 221005, India*

⁵*University of California - Riverside, Riverside, CA 92521, USA*

⁶*China Institute of Atomic Energy (CIAE), Beijing, People's Republic of China*

⁷*Center for Nuclear Study, Graduate School of Science, University of Tokyo, 7-3-1 Hongo, Bunkyo, Tokyo 113-0033, Japan*

⁸*Columbia University, New York, NY 10027 and Nevis Laboratories, Irvington, NY 10533, USA*

⁹*Florida State University, Tallahassee, FL 32306, USA*

¹⁰*Georgia State University, Atlanta, GA 30303, USA*

¹¹*Hiroshima University, Kagamiyama, Higashi-Hiroshima 739-8526, Japan*

- ¹²*Institute for High Energy Physics (IHEP), Protvino, Russia*
¹³*Iowa State University, Ames, IA 50011, USA*
¹⁴*KEK, High Energy Accelerator Research Organization, Tsukuba-shi, Ibaraki-ken 305-0801, Japan*
¹⁵*Korea University, Seoul, 136-701, Korea*
¹⁶*Russian Research Center "Kurchatov Institute", Moscow, Russia*
¹⁷*Kyoto University, Kyoto 606, Japan*
¹⁸*Lawrence Livermore National Laboratory, Livermore, CA 94550, USA*
¹⁹*Los Alamos National Laboratory, Los Alamos, NM 87545, USA*
²⁰*Department of Physics, Lund University, Box 118, SE-221 00 Lund, Sweden*
²¹*McGill University, Montreal, Quebec H3A 2T8, Canada*
²²*Institut für Kernphysik, University of Münster, D-48149 Münster, Germany*
²³*Myongji University, Yongin, Kyonggido 449-728, Korea*
²⁴*Nagasaki Institute of Applied Science, Nagasaki-shi, Nagasaki 851-0193, Japan*
²⁵*University of New Mexico, Albuquerque, NM 87131, USA*
²⁶*New Mexico State University, Las Cruces, NM 88003, USA*
²⁷*Chemistry Department, State University of New York - Stony Brook, Stony Brook, NY 11794, USA*
²⁸*Department of Physics and Astronomy, State University of New York - Stony Brook, Stony Brook, NY 11794, USA*
²⁹*Oak Ridge National Laboratory, Oak Ridge, TN 37831, USA*
³⁰*PNPI, Petersburg Nuclear Physics Institute, Gatchina, Russia*
³¹*RIKEN (The Institute of Physical and Chemical Research), Wako, Saitama 351-0198, JAPAN*
³²*RIKEN BNL Research Center, Brookhaven National Laboratory, Upton, NY 11973-5000, USA*
³³*Universidade de São Paulo, Instituto de Física, Caixa Postal 66318, São Paulo CEP05315-970, Brazil*
³⁴*SUBATECH (Ecole des Mines de Nantes, IN2P3/CNRS, Universite de Nantes) BP 20722 - 44307, Nantes-cedex 3, France*
³⁵*St. Petersburg State Technical University, St. Petersburg, Russia*
³⁶*University of Tennessee, Knoxville, TN 37996, USA*
³⁷*Department of Physics, Tokyo Institute of Technology, Tokyo, 152-8551, Japan*
³⁸*University of Tokyo, Tokyo, Japan*
³⁹*Institute of Physics, University of Tsukuba, Tsukuba, Ibaraki 305, Japan*
⁴⁰*Vanderbilt University, Nashville, TN 37235, USA*
⁴¹*Waseda University, Advanced Research Institute for Science and Engineering, 17 Kikui-cho, Shinjuku-ku, Tokyo 162-0044, Japan*
⁴²*Weizmann Institute, Rehovot 76100, Israel*
⁴³*Yonsei University, IPAP, Seoul 120-749, Korea*
⁴⁴*KFKI Research Institute for Particle and Nuclear Physics (RMKI), Budapest, Hungary[†]*
(October 24, 2018)

Identified $\pi^{+/-}$, $K^{+/-}$, p and \bar{p} transverse momentum spectra at mid-rapidity in $\sqrt{s_{NN}} = 130$ GeV Au-Au collisions were measured by the PHENIX experiment at RHIC as a function of collision centrality. Average transverse momenta increase with the number of participating nucleons in a similar way for all particle species. Within errors, all mid-rapidity particle yields per participant are found to be increasing with the number of participating nucleons. There is an indication that $K^{+/-}$, p and \bar{p} yields per participant increase faster than the $\pi^{+/-}$ yields. In central collisions at high transverse momenta ($p_T \gtrsim 2$ GeV/c), \bar{p} and p yields are comparable to the $\pi^{+/-}$ yields.

PACS numbers: 25.75.Dw

We report first results on identified $\pi^{+/-}$, $K^{+/-}$, p and \bar{p} production as a function of collision centrality in $\sqrt{s_{NN}} = 130$ GeV Au+Au collisions, measured by the PHENIX experiment at the Relativistic Heavy Ion Collider (RHIC). The PHENIX objective is to search for signatures of deconfinement and chiral symmetry restoration and to study the transition from normal to deconfined nuclear matter by utilizing a wide variety of probes.

Early RHIC results show that the transverse energy density and particle multiplicities are considerably higher than previously observed in relativistic heavy-ion collisions [1,2].

Measured energy densities extend into the region predicted to be favorable for the formation of a quark-gluon plasma [3]. Identified hadron spectroscopy provides a tool for studying reaction dynamics beyond that of global event characterization. The yields of hadrons reflect the particle production mechanism, while spectral shapes are sensitive to the dynamical evolution of the system. The mass and centrality dependence of the spectra can help differentiate between competing theoretical descriptions such as collective hydrodynamical expansion [4,5] or transverse momentum (p_T) broaden-

ing in the partonic stage of the reaction [6]. Additionally the relative yields of baryons and mesons at high ($p_T \simeq 2$ GeV/c) may give insight into baryon number transport [7] and the interplay between soft and hard processes.

The PHENIX detector has diverse particle identification (PID) capabilities [8], including excellent hadron identification over a broad momentum range. This measurement was performed using a portion of the east central-arm spectrometer, covering pseudo-rapidity $|\eta| < 0.35$ and $\Delta\phi = \pi/4$ in azimuthal angle.

The collision z -vertex and the timing system's start signal are generated by the Beam-Beam Counters (BBC); two arrays of quartz Cherenkov radiators which surround the beam axis covering $\eta = \pm(3.0 - 3.9)$. The tracking system includes a multi-layer focusing drift chamber located outside an axially-symmetric magnetic field at a radial distance between 2.0 m and 2.4 m followed by a multi-wire proportional chamber with pixel-pad readout (PC1) [9]. Pattern recognition in the DC is based on a combinatorial Hough transform in the track bend plane [10]. The polar angle of the track is determined by PC1 and the collision z -vertex. A track model based on a field-integral look-up table determines the charged particle momentum and the path length to the time-of-flight (TOF) wall. The momentum resolution is $\delta p/p \simeq 0.6\% \oplus 3.6\% p$ (GeV/c).

The timing system stop signal for each particle is measured by the TOF scintillator wall, located at a radial distance of 5.06 m, resulting in a flight-time measurement with a resolution of $\sigma \simeq 115$ ps. Reconstructed tracks are projected to the TOF and matched with hits in the scintillator slats using a momentum-dependent search window determined by multiple scattering and the momentum resolution. A velocity dependent energy loss cut based on a Bethe-Bloch parameterization is applied to the measured TOF pulse height. Combining the momentum and flight-time, we reconstruct the particle mass and select particles by applying 2σ momentum dependent cuts in mass-squared.

Corrections for geometrical acceptance, decay-in-flight, momentum resolution and reconstruction efficiency are determined using a single-particle full GEANT Monte Carlo (MC) simulation. The acceptance correction assumes that the spectra are flat in azimuth and in rapidity for $|y| < 0.5$ [11]. Fiducial area cuts, energy loss and hit-track matching cuts are applied consistently in simulation and data. In peripheral events the track reconstruction efficiency is $\approx 98\%$. As the centrality increases, the efficiency is reduced due to the increased detector occupancy. Multiplicity dependent corrections are obtained by embedding simulated tracks into real events. Track-by-track corrections are applied taking into account the event centrality and the particle species. The efficiency for $\pi^{+/-}$ in the most central events is $\approx (68 \pm 6)\%$, independent of momentum. In the case of overlapping

hits in the TOF wall, the earliest pulse reaching each photo-multiplier is recorded. This favors the faster particles; hence, in central events heavier particles suffer an additional reconstruction inefficiency of $\approx 4\%$. Corrections for feed-down from weak decays are not applied. A MC simulation is used to estimate the probability for reconstructing protons from Λ decays as prompt protons. Within the PHENIX acceptance this probability is $\approx 50\%$ at $p_T = 0.5$ GeV/c, $\approx 32\%$ at $p_T = 1$ GeV/c and $\approx 12\%$ at $p_T \geq 2$ GeV/c. Taking $\frac{\Lambda}{p} = 1$ as an upper limit, we estimate 33% as the upper limit of weak decay contribution to the reported p, \bar{p} yields and maximal 16% change of measured $\langle p_T \rangle$.

About 140,000 minimum bias events, representing $92 \pm 4\%$ of the total inelastic cross-section of 6.8 b [1] were analyzed. This sample was subdivided into five centrality classes: 0 – 5%, 5 – 15%, 15 – 30%, 30 – 60% and 60 – 92%, using the BBC and Zero-Degree-Calorimeters for event characterization [1]. For each class, the average number of nucleons participating in the collision (N_{part}) is obtained from a Glauber model calculation [12].

Fig. 1 shows the invariant yield as a function of p_T for π^+, K^+, p (left panel) and π^-, K^-, \bar{p} for three centrality selections. Error bars in the figure are the combined statistical errors in the data and the corrections. Systematic uncertainties from acceptance, multiplicity-dependent efficiency corrections and PID cuts result in an overall systematic error in the absolute normalization of $\approx 11\%$ for all species. As a consistency check, we have added all identified charged hadron spectra in the p_T region where PID is available for all species and compared to the PHENIX charged hadron measurement [12]. The results agree to better than 10% for all centralities. Additionally, the PHENIX π^0 spectra [12] and the $\pi^{+/-}$ spectra in the region of overlapping p_T are within $\approx 10\%$ for the central and $\approx 25\%$ for the peripheral selections, which is within the systematic errors of the two measurements. \bar{p} results presented here are also in agreement (within errors) with recent publication [13].

In peripheral events the $\pi^{+/-}$ spectra exhibit a concave shape, well described by a power-law parameterization as observed in hadron-hadron collisions [14]. With increasing centrality the curvature in the spectra decreases, leading to an almost exponential dependence on p_T for the most central events. Over the measured p_T range, the $K^{+/-}$ spectra can be described by an exponential distribution either in p_T or in $m_T = \sqrt{p_T^2 + m^2}$, while the p and \bar{p} spectra can be described either as a Boltzmann or an exponential distribution in m_T . The slopes of the m_T spectra flatten and the mean transverse momentum ($\langle p_T \rangle$) increases with particle mass and with centrality. This behavior has been previously observed in lower energy heavy ion collisions at the BNL-AGS [15] and at the CERN-SPS [16,17] and was attributed to collective radial motion (flow).

At lower energies, it is not uncommon for the proton yields to equal or exceed the π^+ yields, since many of the protons come from the initial state. A new feature observed for the first time at RHIC is that in central collisions at $p_T \approx 2 \text{ GeV}/c$ the \bar{p} yields are comparable to the π^- yields. Positive and negative hadrons behave in a similar way. In central events the proton yields approach the π^+ spectra around $p_T \simeq 1.6 \text{ GeV}/c$. As the centrality decreases, this happens at larger p_T . In peripheral events, p and \bar{p} spectra are below the $\pi^{+/-}$ spectra over the whole measured p_T range. Since anti-protons are not as numerous as the protons, \bar{p} and π^- yields become comparable only at the high end of the measured pion p_T range in the most central collisions. We note that in pp [18] and $p\bar{p}$ [19] collisions at $\sqrt{s} = 23 - 63 \text{ GeV}$ and $\sqrt{s} = 300 - 1800 \text{ GeV}$ respectively, the \bar{p}/π^- ratio steadily increases with p_T up to $\simeq 0.33$ at $p_T \simeq 1.5 \text{ GeV}/c$ nearly independent of \sqrt{s} . Data on baryon/meson ratios at higher p_T are only available from pp collisions at ISR energies ($\sqrt{s} = 23 - 63 \text{ GeV}$) and show that above $p_T \simeq 1.5 \text{ GeV}/c$ the \bar{p}/π^- ratio rises to $\simeq 0.4$ at $p_T \simeq 2 \text{ GeV}/c$ and then drops, as expected if valence quark jet fragmentation is the dominant production mechanism for high p_T hadrons. In central collisions at RHIC the high p_T (anti)proton/pion ratios are ~ 1 - much larger than in pp collisions.

Hydrodynamic calculations with fixed freeze-out temperature [5] or with freeze-out modeled using a hadronic cascade [4] suggest that hydrodynamic expansion is responsible for the baryon dominance at high p_T . However, protons/anti-protons produced via a baryon junction mechanism combined with jet-quenching in the pion channel are shown to exhibit the same effect [7]. Intrinsic p_T broadening in the partonic phase caused by gluon saturation [6] gives yet another alternative explanation. The above models have similar predictions in the p_T range measured here, but show different behavior at higher p_T . New data with broader p_T range is needed in order to distinguish between currently available theories.

To quantify the centrality and mass dependencies of hadron production, we determine the mean ($\langle p_T \rangle$ shown in Fig. 2) and the integral (dN/dy shown in Fig. 3) of the p_T distributions. Both quantities require extrapolation of the spectra below and above the measured range. For each particle species, we use at least two functional forms consistent with the data, as outlined above and the results presented are averaged between two fits. The fraction of the yield in the extrapolated regions is estimated $30 \pm 6\%$ for $\pi^{+/-}$, $40 \pm 8\%$ for $K^{+/-}$ and $25 \pm 7.5\%$ for p/\bar{p} . Combining systematic uncertainties in the extrapolation fractions and the estimated background under mass-squared peaks (2%, 5% and 3%) yield systematic uncertainties in the measured $\langle p_T \rangle$ of 7%, 10% and 8% for $\pi^{+/-}$, $K^{+/-}$ and p/\bar{p} , respectively. Further combining the above uncertainties, which only affect the shape of the spectra, with the 11% uncertainty in the abso-

lute normalization gives systematic uncertainties of 13%, 15% and 14% in the measured dN/dy for $\pi^{+/-}$, $K^{+/-}$ and p/\bar{p} , respectively. We note that after converting to $dN/d\eta$, the sum of the identified charged hadron yields agrees with the previously published PHENIX results on total charged multiplicity $dN_{ch}/d\eta$ [1] within 5%.

Fig. 2 shows the $\langle p_T \rangle$ as a function of N_{part} for π^+, K^+, p (left panel) and π^-, K^-, \bar{p} . Filled points are this measurement; open points at $N_{part} = 2$ are interpolations to $\sqrt{s} = 130 \text{ GeV}$ obtained from pp and $p\bar{p}$ data at lower [18] and higher energies [19], respectively. In peripheral Au-Au collisions at RHIC $\pi^{+/-}$ and $K^{+/-}$ exhibit similar $\langle p_T \rangle$ to those in pp collisions, but protons and anti-protons have significantly higher $\langle p_T \rangle$, indicating that nuclear effects are important even at small N_{part} . For all measured particles species, $\langle p_T \rangle$ increases by $\approx 12 - 14\%$ from the first to the second centrality bin (i.e. N_{part} 14 to 79). Above $N_{part} = 100$ the $\pi^{+/-}$ and $K^{+/-}$ $\langle p_T \rangle$ appear to saturate, whereas the p and \bar{p} $\langle p_T \rangle$ rises slowly. However, we note that going from peripheral to the most central event class the overall increase in $\langle p_T \rangle$ is $\approx 20 \pm 5\%$ independent of particle species.

Fig. 3 shows the yields per participant versus N_{part} . Error bars include statistical and multiplicity dependent systematic errors. Systematic uncertainties in N_{part} that can move all curves independent of mass are shown with bands around the positive hadron points. Total systematic uncertainties in N_{part} and the yields at each N_{part} are listed in Table I.

For all particle species, the yield per participant increases with N_{part} . As for $\langle p_T \rangle$, most of the increase occurs between the two most peripheral centrality selections (i.e. N_{part} 14 to 79). However, in contrast with the centrality dependence of $\langle p_T \rangle$, we see an indication that the total increase in the yields per participant differs among particle species as we go from peripheral to central events. The pion yield per participant rises by $21\% \pm 6\%(stat) \pm 8\%(syst)$. The kaon yields per participant rise faster: $94\% \pm 11\%(stat) \pm 26\%(syst)$ and $66\% \pm 12\%(stat) \pm 20\%(syst)$, for K^+ and K^- , respectively. Similar trends in the centrality dependence of strangeness production have been observed in lower energy heavy ion collisions at the BNL-AGS [20] and at the CERN-SPS [17]. It is interesting to note that at RHIC p and \bar{p} yields per participant behave similarly to the $K^{+/-}$ yields and also rise faster than the pions with increasing N_{part} . The increase is $58\% \pm 5\%(stat) \pm 16\%(syst)$ and $72\% \pm 9\%(stat) \pm 20\%(syst)$, respectively. The similar centrality dependence in p and \bar{p} yields per participant indicates that baryon/anti-baryon pair production is the dominant source of protons and anti-protons alike.

In heavy ion collisions at AGS energies [22] the \bar{p} production is close to threshold, the yields per participant are lower than in pp collisions and decrease from peripheral to central collisions, probably due to annihilation.

At the SPS, the \bar{p} yield per participant is larger than the pp value and has almost no centrality dependence [23]. At RHIC, the total yield of anti-protons at mid-rapidity in central Au-Au collisions is a factor of $\simeq 1000$ larger than at the AGS [22] and nearly an order of magnitude above that in Pb+Pb collisions at CERN [24]. Most of the increase is due to the \sqrt{s} dependence of baryon/anti-baryon pair production, however the yield per participant rises noticeably from peripheral to central collisions.

In conclusion, an intriguing new behavior in identified hadron production at RHIC is reported. In central Au-Au collisions the anti-protons yield is comparable to the π^- at high p_T - a behavior never observed before in elementary or in heavy-ion collisions. $\langle p_T \rangle$ rises with centrality similarly for all particle species, while $K^{+/-}$, p and \bar{p} yields per participant increase somewhat faster than the $\pi^{+/-}$ yields.

We thank the staff of the Collider-Accelerator and Physics Departments at BNL for their vital contributions. We acknowledge support from the Department of Energy and NSF (U.S.A.), MEXT and JSPS (Japan), RAS, RMAE, and RMS (Russia), BMBF, DAAD, and AvH (Germany), VR and KAW (Sweden), MIST and NSERC (Canada), CNPq and FAPESP (Brazil), IN2P3/CNRS (France), DAE and DST (India), KRF and CHEP (Korea), the U.S. CRDF for the FSU, and the US-Israel BSF.

* Deceased

† Not a participating Institution.

- [1] K. Adcox *et al.*, Phys. Rev. Lett. **86**, 3500 (2001);
 [2] K. Adcox *et al.*, Phys. Rev. Lett. **87**, 052301 (2001);
 B.B. Back *et al.*, Phys. Rev. Lett. **85**, 3100 (2000);
 C. Adler *et al.*, Phys. Rev. Lett. **87**, 112303 (2001).
 [3] e.g. see *Proc. Quark Matter 1984*, ed. K. Kajantie (Springer, Berlin 1985); *Proc. Quark Matter 1987*, eds. H. Satz, H. J. Specht, R. Stock, Z. Phys. **C38**, 1-370 (1988).
 [4] D. Teaney *et al.*, Phys. Rev. Lett. **86**, 4783 (2001); nucl-th/0110037.
 [5] P. Kolb *et al.*, Nucl. Phys. **A696**, 197 (2001); P. Huovinen *et al.*, Phys. Lett. **B503**, 58 (2001)
 [6] J. Schaffner-Bielich *et al.*, hep-ph/0101133; nucl-th/0108048 and references therein.
 [7] I. Vitev and Miklos Gyulassy, nucl-th/0104066.
 [8] H. Hamagaki (PHENIX Collaboration), Nucl. Phys. **A698**, 412c (2002).
 [9] J. Velkovska, Proc. CAARI 2000, AIP **CP576**, 227 (2001).
 [10] J. T. Mitchell *et al.*, Nucl. Instrum. Methods **A482**, 498-515 (2002)
 [11] B.B. Back *et al.*, Phys. Rev. Lett. **87**, 102303 (2001).
 [12] K. Adcox *et al.*, Phys. Rev. Lett. **88**, 22301 (2002)

- [13] C. Adler *et al.*, Phys. Rev. Lett. **87**, 262302 (2001).
 [14] C. Albajar *et al.*, Nucl. Phys. **B335**, 261 (1990).
 [15] L. Ahle *et al.*, Nucl. Phys. **A610**, 139c-152c (1996).
 [16] I.G. Bearden *et al.*, Phys. Rev. Lett. **78**, 2080 (1997).
 [17] J. Bachler *et al.*, Nucl. Phys. **A661**, 45c-54c (1999).
 [18] B. Alper *et al.*, Nucl. Phys. **B100**, 237-290 (1975).
 [19] T. Alexopoulos *et al.*, Phys. Rev. **D48**, 984 (1993).
 [20] L. Ahle *et al.*, Phys. Rev. **C59**, 2173 (1999); Phys. Rev. **C60**, 044904 (1999).
 [21] J. Barrette *et al.*, Phys. Rev. Lett. **70**, 1763 (1993)
 [22] D. Beavis *et al.*, Phys. Rev. Lett. **75**, 3633 (1995);
 M. Bennett *et al.*, Phys. Rev. **C56**, 1521 (1997);
 L. Ahle *et al.*, Phys. Rev. Lett. **81**, 2650 (1998).
 [23] G. I. Veres, Nucl. Phys. **A661**, 383c-386c (1999).
 [24] I.G. Bearden *et al.*, Phys. Lett. **B388**, 431-436 (1996).

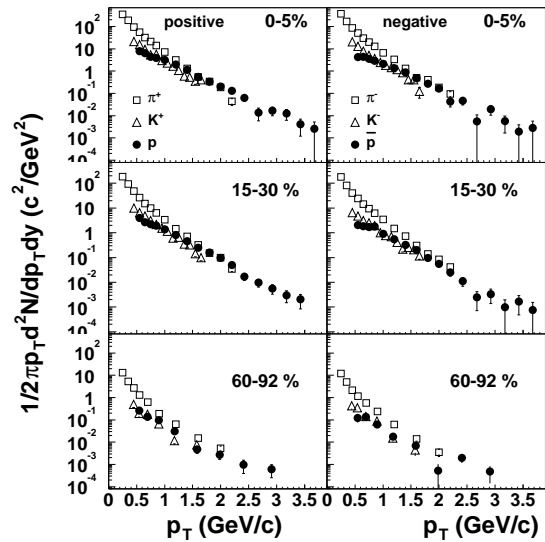


FIG. 1. Transverse momentum spectra measured at mid-rapidity for π^+ , K^+ , p (left) and π^- , K^- , \bar{p} at the three different centrality selections indicated in each panel. The symbols indicated in the top panels apply for all centrality selections.

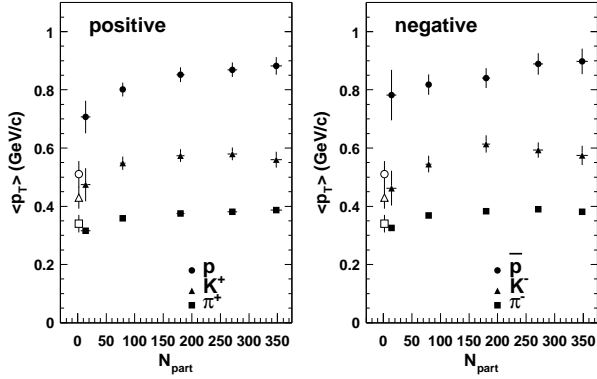


FIG. 2. Average transverse momentum for π^+ , K^+ , p (left) and π^- , K^- , \bar{p} as a function of the number of nucleons participating in the collision N_{part} . The error bars represent the statistical errors. The systematic errors are discussed in the text. The open points are interpolations from pp and $p\bar{p}$ data, see text for details.

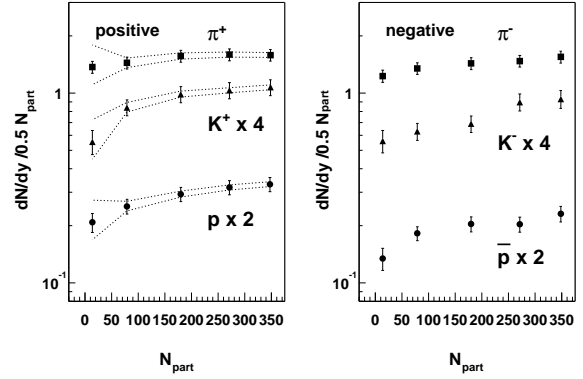


FIG. 3. $dN/dy|_{y=0}$ per participant for π^+ , K^+ , p (left) and π^- , K^- , \bar{p} as a function of N_{part} . The error bars include statistical and systematic errors in dN/dy . The dashed lines around the positive hadrons show the effect of the systematic error on N_{part} which affects all curves in the same way.

TABLE I. Integrated hadron (π^\pm , K^\pm , p and \bar{p}) yields at mid-rapidity for five centrality classes (see text) identified by the indicated number of participants N_{part} . The errors on N_{part} are the systematic errors. The errors listed for $\langle dN/dy|_{y=0} \rangle$ are statistical. The systematic errors are 13%, 15% and 14% for π^\pm , K^\pm , p and \bar{p} , respectively.

N_{part}	348 ± 10.0	271 ± 8.4	180 ± 6.6	79 ± 4.6	14 ± 3.3
π^+	276 ± 3	216 ± 2	141 ± 1.5	57 ± 0.6	9.6 ± 0.2
π^-	270 ± 3	200 ± 2	129 ± 1.4	53.3 ± 0.6	8.6 ± 0.2
K^+	46.7 ± 1.5	35.0 ± 1.3	22.2 ± 0.8	8.3 ± 0.3	0.97 ± 0.11
K^-	40.5 ± 2.3	30.4 ± 1.4	15.5 ± 0.7	6.2 ± 0.3	0.98 ± 0.1
p	28.7 ± 0.9	21.6 ± 0.6	13.2 ± 0.4	5.0 ± 0.2	0.73 ± 0.06
\bar{p}	20.1 ± 1.0	13.8 ± 0.6	9.2 ± 0.4	3.6 ± 0.1	0.47 ± 0.05